South African Journal of Chemical Engineering 44 (2023) 89–102

Contents lists available at ScienceDirect

South African Journal of Chemical Engineering

journal homepage: www.elsevier.com/locate/sajce

Statistical analyses of pore radii on the performance of PET-nanocomposite membranes in the removal of iron and anions from Ibeshe River

Oluranti Agboola [a,*], Ajibola Ademola Khalih [a], Olagoke Oladokun [a], Augustine Omoniyi Ayeni [a], Frederick Chukwudubem Uzokwe [a], Olayemi Odunlami [a], Francis Elehinafe [a], Abdulrazaq Yahaya [b], Ojo Sunday Isaac Fayomi [c]

[a] Department of Chemical Engineering, Covenant University, Ota, Ogun State, Nigeria
[b] Department of Pure and Industrial Chemistry, Kogi State University, Anyigba, Kogi State, Nigeria
[c] Department of Mechanical and Biomedical Engineering, Bells University of Technology, Ota, Ogun State, Nigeria

ARTICLE INFO

Keywords:
PET-nanocomposite membranes
SEM
ImageJ
Python
Pore radius
Data distribution

ABSTRACT

The industrialization in Lagos State has impacted the Ibeshe watershed, as a result, lower water quality is being experienced. Hence, a novel way on the potential use of waste to treat Ibeshe watershed by synthesizing of graphene oxide and incorporating it into PET bottle waste membranes was studied. Polyethylene terephthalate (PET) membranes embedded with 1wt%, 2wt%, and 3wt% graphene oxide (GO) (M1, M2, and M3), were prepared via non-solvent-induced phase separation on polyester nonwoven support with the use of polyethylene glycol (PEG) as an additive. The surface morphologies of the three membranes appeared to be considerably different. The pore volume steadily reduces with an upsurge in the quantity of GO embedded in the membranes. A statistical assessment employing a uniform distribution curve was done using Python and the outcomes depict that the distribution of the radius data was firmly gathered around the mean. From the adsorption study, Fe^{2+} does not have the power to attract HCO^{3-} in the transitory state at the surface of the membrane; hence HCO^{3-} could not reach equilibrium at 80 min. The membranes' performance was studied via flux and the rejection of iron and anions. The rejection rate calculated for the three anions and iron was observed to be high in the M3 membrane. The M3 membrane% rejection of the anions and iron is 96%, 85%%, 72%, and 60% for NO^{3-}, Cl^{-}, HCO^{3-} and Fe, respectively. An upsurge in the amount of GO improved the water flux; hence, 3wt% GO gave the maximum water flux.

1. Introduction

Water makes up 60% of the human body and is vital to all life on Earth. 97.5% of the water on the planet's surface is salty, which cannot be utilized directly since 80% of this saltwater is frozen in the icecaps or mixed as soil moisture. Freshwater accounts for the remaining 2.5%, which is supposed to be sufficient to provide for all life on Earth. Unfortunately, this water is not evenly distributed globally and is not accessible in abundant quantities when and where it is needed. Most of the available water is heavily polluted by agricultural and industrial waste and cannot be consumed, so the key issues that need to be addressed are water quality and quantity (Bethi et al., 2016). One of the most important environmental challenges is the contamination of rivers, streams, and wetlands with toxins. There is a great deal of damage caused by waterborne chemical waste entering rivers, streams, and ponds. As rain falls and penetrates the rock, it usually dissolves some of the iron at varying concentrations. The rain transports the iron along with it as it continually penetrates through the rock and soil. With time, this rainwater moves into groundwater or goes into sources of freshwater such as lakes and rivers; which could come to be part of the local water supply. Some municipal water systems get their water supply from these sources; this could culminate in high levels of iron in their water, and the filters used by the Municipal to eliminate bacteria and other detrimental pollutants might not filter it out at all times. In addition to that, wells that take water from aquifers that have iron content might also contain high iron concentrations. Generally, iron in water is of one of two forms; ferrous iron, which is soluble in water, and ferric iron, which is insoluble in water. Typically, water that contains ferrous iron is

* Corresponding author.
E-mail address: oluranti.agboola@covenantuniversity.edu.ng (O. Agboola).

https://doi.org/10.1016/j.sajce.2023.01.011
Received 16 May 2022; Received in revised form 23 August 2022; Accepted 29 January 2023
Available online 31 January 2023

naturally faint from pure water owing to the fact that the iron is uniformly dissolved in the water; hence, the water will remain clear. Nonetheless, when the water eventually gets to a home well tank or pours out into the air, the iron will be oxidized and turns into insoluble ferric iron. As a result, the iron will then be visible and starts to affect water quality (Longs Ecowater 2022). Presently, the endorsed limit for iron in water is 0.3 mg/l (ppm). This is centered on appearance and taste rather than on any damaging health consequence (Department of natural resources 2017). In addition to iron, there are different anions in river water.

Wastewater from all over; rain, households, industries, non-domestic sources and groundwater along the Abuja axis in Ikorodu all flow to the same place, the Ibeshe River. Ibeshe River water contains iron which has deteriorated the river water beyond acceptable levels due to uncontrolled discharge of rainwater, untreated wastewater and solid debris into the river. The development and industrialization of Ikorodu's Ibeshe watershed also contributed to the low quality of water, affecting the aquatic ecosystem and downstream users. This has increased the scarcity of water in that area of Lagos, in spite of its proximity to water, Lagos has limited access. Currently, the city's water demand per day is greatly beyond the production by the municipal utility Lagos Water Corporation. In addition, the utility does not even provide half of the needed amount of water per day; which is 540 million gallons, leaving Lagos with an enormous water shortage of about 320 million gallons (Oluwafemi 2018).

There are numerous ways of treating wastewater, and many techniques for wastewater treatment have been developed; such methods include reverse osmosis (Yang et al., 2016), ion exchange (Beita-Sandí et al. 2017), gravity (Carr et al., 2016) and adsorption, among others. As a result of its cheap cost and flexibility, adsorption is widely utilized to remove contaminants from water. Adsorbents of various types, such as polymer nanocomposites, activated carbon, and magnetic nanoparticles, may be used in the treatment of wastewater. They may assist in the removal of harmful pollutants such as heavy metals, even when used in little amounts. Despite the fact that adsorption can remove the vast majority of pollutants from water, it is subject to a number of limitations, including a scarcity of suitable adsorbents with high adsorption capacity and a ban on their commercial usage (Gaouar et al. 2016). This is why more effective methods such as membrane technology are required.

Nanocomposite membranes are considered collections of innovative filtration materials that are made of nanofillers dispersed in a polymeric or inorganic oxide matrix prior to casting o functionalize them. The modification of nanocomposite membranes is considered advanced membranes technology because it enhances the treatment of water and wastewater as a result of the properties of nanomaterials embedded in the membranes. The integration of nanofillers usually changes the membrane properties by improving its separation performance, improving its pore structure and permeability, stabilizing flux, and it gives the impression of an anti-fouling behavior (Younas et al., 2017; Wu et al., 2018). Particles contained in the fluid interrelate with the membranes physically or chemically for all filtration modes, resulting in membrane fouling, which is the process in which foulants are deposited on the surface of the membrane or within the pores. Membrane fouling ensues via three main mechanisms: (1) adsorption, which is a mass deposit process in which small particles stick to the pore walls and then shrink the pore active radius; (2) blocking, which is a separate process in which particles that are larger than pores incompletely or entirely cover the ingress of a pore; and (3) caking, is the process in which an added stratum of porous medium, consists of the particles transported by the flow, forms on top of the membrane surface towards the end of filtration (Gu et al., 2020).

The dispersion of nanofillers in membranes to form nanocomposites used for membrane separation processes not only improves membrane properties but also magnifies the technological possibilities of treating different kinds of wastewater. Different types of nanoparticles have been used to enhance membrane performance; however, literature has recently documented that inorganic nanoparticles could have the capability of being utilized as fillers for the enhancement of microporous ultrafiltration (UF) membranes properties (Luo et al., 2011; Zhao et al., 2012; Li et al., 2016). The properties that are envisaged to be enhanced are water permeability, mechanical and thermal properties together with fouling propensity, in as much as the quantity of nanoparticles dispersed in the polymer was not in excess. Titanium dioxide (TiO_2) nanoparticle is among the most studied inorganic nanoparticles utilized for the preparation of nanocomposite membranes (Khalifa et al., 2021). Another inorganic nanoparticle that is most studied is the graphene oxide (GO) nanoparticles. The utilization of graphene oxide for synthesizing nanocomposite membranes could be designed in two ways (Zinadini et al., 2014). The first way is the direct employment of graphene oxide as a separating stratum (Huang et al., 2014; Li et al. 2021) while the second one is the integration of graphene oxide in a polymer matrix for the enhancement of the membrane performance (Tran et al., 2021). Apart from the methods of integrating graphene oxide in membranes; there are also different methods of synthesizing graphene oxides, these methods also have effects on membranes performance. Sali et al. (2019) studied the influence of GO synthesis methods on features and performance of polysulfone-graphene oxide mixed matrix membranes for the removal of oil from an oil-water emulsion. The GO used in their study was synthesized through the Hummers', Tour, and Staudenmaier methods. Their study showed that GO synthesized via the Staudenmaier method exhibited a higher concentration of the more polar carbonyl group, which resulted in the upsurge of the membrane hydrophilicity and porosity compared to GO synthesized via the Hummers' and Tour methods. Conversely, the GO synthesized via Hummers' and Tour methods exhibited a larger sheet size, and they are more effectual in improving the mechanical properties of the polysulfone membrane.

Membrane properties like hydrophilicity, roughness, and surface charge have mostly been considered an important aspect in membrane fouling and flux decline. Furthermore, surface modification techniques such as coating are also utilized to enhance high potential membrane. Kim et al. (2009) investigated the effect of surface modifying macromolecules on the properties of poly(ether sulfone) ultrafiltration membranes. Through the addition of surface modifying macromolecules, glass transition temperature reduced and membrane pore size improved. This group also studied the relationship connecting the surface structure and the separation performance of poly(ether sulfone) ultra-filtration membranes when surface modifying macromolecules is incorporated with the membranes. A thorough assessment of the surface free energy established that the hydrophilic surface ensued from strong Lewis base (solid)–acid (liquid) interaction while the hydrophobic surface ensued from the weak Lifshitz–van der Waals interaction (Kim et al., 2010). The authors further worked on the innovative design and synthesis of membranes with silver integrated surfaces to reveal and stimulate new avenues for applied basic functions (Kim et al., 2012).

In addition, researchers recently focused on the utilization of polymer materials that are cost-effective as an alternative polymer for the preparation of membranes. The notion of employing waste as a precursor for the fabrication of membranes has the capacity to assist in curbing the disposal of waste in our environment while offering a smart, low-cost means of utilizing fossil-based polymers as membrane material (Goh et al., 2021). Furthermore, substitutes to conventional polymers resulting from fossil fuels are desired, as the processing of fossil-based polymers is associated with fossil resource depletion and it is also connected to human toxicity, marine eco-toxicity, and global warming as a result of the volatile emission (Patel et al. 2001; Mansoori et al., 2020). With regards to these threats, there has been increasing research interest in employing polymers derived from waste (like chitosan, cellulose, keratin, and rubber) as substitutes for synthesizing membranes.

The thermodynamic compatibility of nanofillers and polymers is key when preparing a nanocomposite. GO sheets are comprehensively oxygenated graphene (with relevant functional groups; i.e. ketones,

epoxide, hydroxyl, diols, and carboxyls functional groups) that have the capacity to significantly change the van der Waals interactions and be more compatible with organic polymers (Marakova et al. 2019; Liang et al., 2020; Lawal 2020). Different studies have been conducted on research on thermodynamics of polymer blends (Rana et al., 1996). For this reason, the miscibility of polymer blends or polymers with nano-fillers is of significant interest to different industries and academia (Rana et al., 1993; Rana et al., 2000). With respect to thermodynamic terms, two components are considered miscible should they form a single-phase system at the level of molecularity (Gadde 1999; Agboola and Sadiku 2014). In addition, thermodynamic interaction of the polymer nano-blends and nanocomposites membranes can be characterized by the rules that govern miscible characteristics of polymer blends; which are understood with respect to thermodynamics vis Gibbs free of mixing. However, the theoretical basis for the comprehension of the polymer solution was first developed in 1942 by Flory and Huggins by independently introducing a model to compute the enthalpy and entropy of mixing polymers in solution (Flory 1942). Nonetheless, there have been subsequent developments to extend the application of the first Flory and Huggins theory to enhance the agreement between the results from theory and experiments. Flory and Krigbaun (1950) invented a thermodynamic theory for dilute polymer solutions while Koningsveld et al. (1974) enhanced the agreement first Flory and Huggins theory with the data obtained from the experiment by using an empirical modification to include composition dependence and give a justification for polydispersity in order to understand polymer compatibility with regards to thermodynamic stability.

With respect to polyethylene terephthalate (PET) and GO, some researchers have also studied the thermodynamic compatibility of PET and GO. Bayat et al. (2019), invented epoxy adhesives using recycled PET, ground rubber tire (GTR), and GO nanoflakes for the study of thermal and mechanical properties. From their study, the adhesive formulations were investigated for tensile and single-lap shear strength, used at the interface between epoxy/carbon fiber and stainless steel through the alteration of the quantity of PET and GO nanosheets. The authors specified and selected the best and the poorest samples with respect to mechanical strength for thermal degradation analyses based on thermogravimetric analysis (TGA). The study showed that the introduction of GO to the adhesive enhanced the thermal stability of epoxy/ (PET/GTR). Zhang et al. (2010) synthesized PET/graphene nanocomposites through melt compounding. The integration of graphene greatly enhanced the electrical conductivity of PET, which subsequently results in a sharp transition from an electrical insulator to a semiconductor. High electrical conductivity of 2.11 S/m was attained with 3.0 vol.% of graphene. The low percolation threshold and higher electrical conductivity were accredited to the high aspect ratio, large specific surface area, and evenly dispersal of the graphene nanosheets in the PET matrix. These studies have shown that GO is compatible with PET with respect to thermal stability and electrical conductivity.

The novelty and research gap of this study is on the potential use of waste to treat wastewater by synthesis of graphene oxide and incorporating it into PET bottle waste as a source material for membrane fabrication to treat wastewater. The motivation for using graphene oxide was its favourable characteristics like hydrophilicity, large surface area and mechanical stability; thus it was envisaged that the mechanical stability of graphene oxide will improve the mechanical property of the waste PET. In addition, the role of GO in the PET membrane was to provide high-flux and energy-efficient membranes for precise ionic and molecular sieving in a bulk solution containing anions and cations. Hence, the main focus of this investigation is to study the impact of pore size variations that ensued from the synthesis of PET-graphene oxide nanocomposite membranes in evaluating their performance in terms of flux and rejection for the removal of pollutants such as iron and anions from the Ibeshe river. In order to enhance the size of the GO nanoparticle, a modified Hummer's method (Paulchamy et al., 2015) would be used for the GO synthesis. Literature also documented that larger nanoparticles sometimes adhered to the exterior of the membrane which will cause minimal disruption. It is hence envisaged that GO produced by a modified Hummer's method would enhance the pore size of the membranes (Dunning 2020). The nanocomposite membranes would therefore be characterized by using SEM to evaluate the pore size distribution and morphology of the membranes.

2. Materials and method

2.1. PET material

Polyethylene terephthalate (PET) was obtained from waste plastic bottles. Polyethylene glycol (PEG-600), dichloromethane (DCM), trifluoroacetic acid (TFA), graphite powder, Hydrochloric acid (HCL), phosphoric acid (H_3PO_4), Sulfuric acid (H_2SO_4), potassium permanganate (KM_nO_4) are reagents and chemical used for this study. They are analytical grade reagents and gotten from Sigma-Aldrich.

2.2. Graphene oxide synthesis

The utilization of nanomaterials for the fabrication of nanocomposite membranes has established its uses to be an outstanding antifouling resistance (Agboola et al., 2021). Graphene oxide was synthesized from pure graphite powder of 20 μm by employing a modified Hummer's method (Paulchamy et al., 2015). A 9:1 ratio of sulfuric acid (H_2SO_4) to phosphoric acid (H_3PO_4) was used; the solution was then mixed with 0.225 g graphite powder. 1.32 g potassium permanganate was then gradually added (dropwise) to the solution ($KMnO_4$) and subjected to 6 h agitation using a stirrer. After 6 h of agitation, 1 mL hydrogen peroxide (H_2O_2) was progressively added and stirred for 10 min to remove excess $KMnO_4$. An exothermic reaction occurred and subsequently cooled. The solution was centrifuged for 7 min at 5000 rpm using an Eppendorf Centrifuge 5430R, 10 mL of HCl and 30 mL of distilled water were added. The supernatant was then decanted away and the residuals were rewashed trice with HCl and deionized water. A 6 h bake at 125 °C dried the washed GO solution, producing GO powder (Paulchamy et al., 2015). Fig. 1 depicted the synthesized GO oxide from graphite powder.

2.3. Preparation of PET

The PET bottles were first melted to molten and then crushed into sizable bits using an electrical crusher. The sizable bits of the PET were processed to powdery nano sizes using a mechanical grinder. An industrial sieve shaker was used to sieve crushed material off the desired particle size (100 μm) and the remnant is crushed again to obtain the desired particle size.

2.4. Synthesis of PET-graphene oxide nanocomposite membrane

Studies have shown that filtration membranes Embedded with GO possess robust hydrophilicity, molecular selectivity and high chemical stability (Elessawy et al., 2022). The casting solutions method was used in synthesizing the PET-graphene oxide nanocomposite membranes. 20 g of PET was dissolved in trifluoroacetic acid and dichloromethane in a ratio of 1:2 and the solution was stirred for 1 h at room temperature (25 °C) with a magnetic stirrer until it became homogenous. In order to enhance the membrane's performance, polyethylene glycol was continuously added as an additive in dropwise while stirring until the solution was fully clear and homogenous at around 90 min. The resulting polymer solutions were kept at room temperature without being stirred to eliminate trapped air bubbles in the casting solution (Pulido et al., 2019). The experimental design used for the preparation of the membranes is shown in Table 1.

Non-solvent-induced phase separation (NIPS) was used to produce all flat sheet membranes; a 15 cm by 20 cm glass plate was used to cast the membranes. This was accomplished by pouring the casting solution

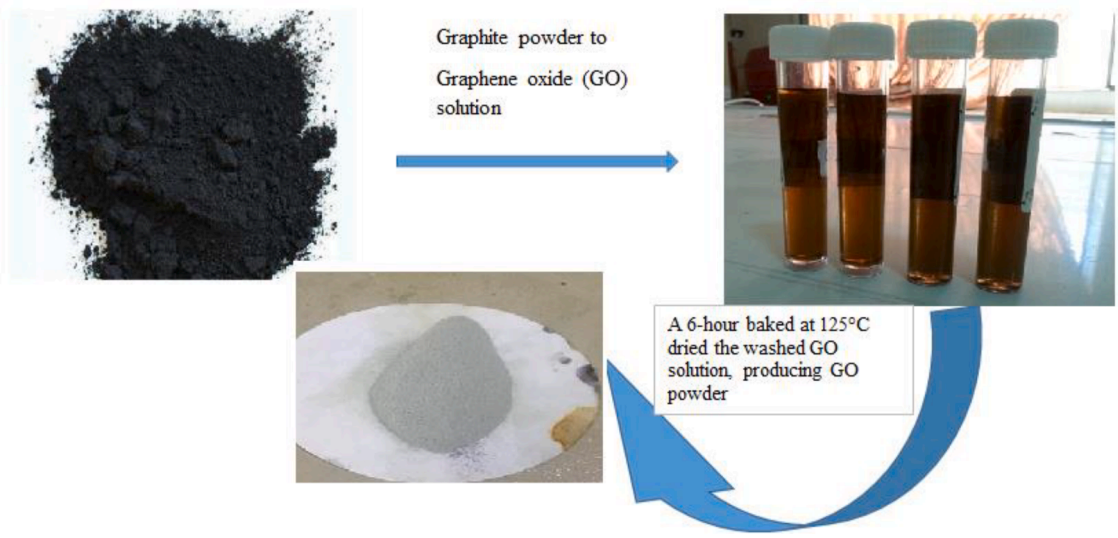

Fig. 1. Pictorial representation of synthesized GO oxide from graphite powder. The GO powder was doped in the PET to synthesize the nanocomposite membrane.

Table 1
Membrane preparation ratios.

Sample	TFA/DCM (wt%)	PET (wt%)	PEG (wt%)	GO (wt%)
M1	72	20	10	1
M2	72	20	10	2
M3	72	20	10	3

over a flat polyester nonwoven fabric set at a room temperature on the casting plate using a casting knife. Immediately thereafter, a thin polymeric film supported on a polyester nonwoven support was separated from the glass. The membranes were cleaned and stored in distilled water.

2.5. Filtration process procedure and mechanism

Fig. 2 displays the schematic representation of the membrane separation process unit that was used for this study. This unit contains a membrane cell which is a stainless steel cell, with a flow in, flow out and pressure pump. The experiments were done at the temperature of 26 °C, a pressure of 0.15 bar, the flow rate of feed into the cell was 12.2 mL/min and the flow rate of the permeate coming out of the cell is between 1 mL/min and 0.08 mL/min. The synthesized nanocomposite membrane was placed inside the membrane cell. The water sample from the Ibeshe River was fed into the membrane cell through the pump with a control panel that was used to control the flow rate of water. The pump outlet hose was connected to the membrane cell inlet and the pump inlet hose was placed in the wastewater tank. The feed was allowed to stabilize for 20 min with all valves closed. The cell pressure pump spun around to upsurge water movement and is powered by a DC electric motor. At every 15 min time interval, the permeate was collected in a beaker by opening the valve at the bottom of the cell and the valve on the top side of the membrane cell was opened so as to collect the retentate. The transport mechanism involves the use of a driving force (pressure pump)

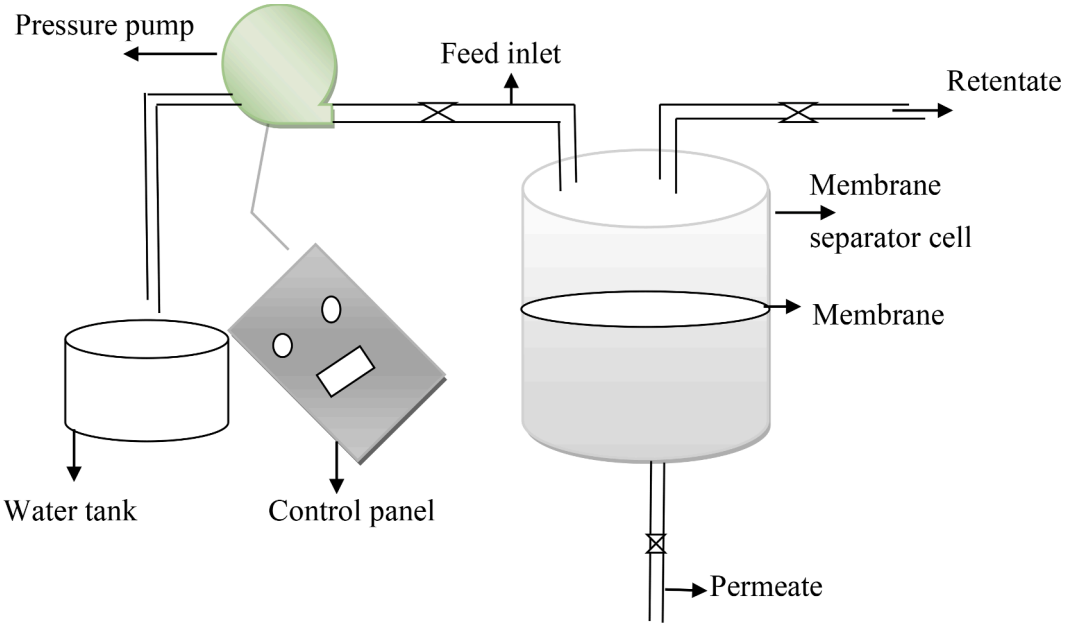

Fig. 2. Schematic representation of the membrane separation unit. The unit comprises of a membrane cell with flow in and flow out together with a pressure pump and attached to it, is the flow control panel.

which forces the feed stream that flows perpendicularly to the membrane surface to move through the membrane. The components retained on the surface of the membrane will accumulate to form a layer of cake, which will result in the reduction of permeate as a result of added resistance to the filtration of the layer of cake (De Meis 2017; Diaz-Reinoso 2020).

2.6. Brunauer-Emmett-Teller (BET)

Any carbon materials can be well analysed knowing the BET surface area as determined by utilizing the analysis of nitrogen adsorption isotherms. BET was used to explain the physical adsorption of gas molecules on the GO surface. The GO surface was characterized by ASAP 2020 V4.02 (V4.02 H) A direct measurement of the specific surface area for the GO was done by gas adsorption through the exposure of the dry GO powder sample to inert gas; which is N_2, under a low-pressure dose of 5.000 cm^3/g to develop an isotherm. The warm free space measured was 27.3220 cm^3, and the cold free space measured was 82.6550 cm^3 was used. The bath analysis temperature of 77.4 K, and an ambient temperature of 295.15 K was set. Preceding the measurement of surface area, the GO sample was degassed under vacuum by manually raising the temperature from ambient to 473.15 K within approximately 30 min, then holding at 473.15 K for 7 h. The degas procedure was done to remove volatiles; which is mainly water, from the surface of the GO powder. The sample was passively cooled back to the ambient temperature and backfilled with N_2, which is the analysis adsorptive gas, after the completion of the degassing procedure. A post-degas mass of GO (0.05 g) was measured for the BRT analysis.

2.7. Scanning electron microscopy (SEM) / Energy dispersive X-Ray (EDX)

The morphological structure of the synthesized PET-graphene oxide nanocomposite membranes was examined with the utilization of SEM. It is a tool commonly used for showing the microstructure of membrane material (Agboola et al., 2014). The SEM equipment employed for the visualization of the surfaces of the membranes was a Joel Field Emission Electron Microscope JESM-7600F. The morphological analysis of the membranes was attained by employing a fast-tracking voltage of 15 kV, working with a low beam mode for preventing the samples from being damaged. The samples prepared were firmly fit in the specimen chamber of the microscope, coated with a platinum coating of electrically conducting material via the deposition of the coating material on the sample employing a low vacuum sputter or high vacuum evaporation.

2.8. Theory

ImageJ is a Java-based image processing program technologically established at the National Institutes of Health and the Laboratory for Optical and Computational Instrumentation. It is an open-source software that facilitates the processing and analysis of scientific images. For the purpose of this work, the data used for statistical study was generated using ImageJ Software.

Python software was used to statistically analyze the data extracted from ImageJ. The pore radius extracted from ImageJ was analyzed using Quartiles analysis using a NumPy. It is part of descriptive statistics that gives a better understanding of the data at hand. Quartiles analysis was used to understand the central tendency which is a solitary value that makes an effort to pronounce a set of data by detecting the central position contained within the set of data. Then, this analysis should have the capacity of predicting the precise porosity of membrane microstructures for diverse sets of input parameters. Through the variation of pore sizes and the number of sites (n) can be located. An additional input variable that can be used to analyze pores of membrane from the structural morphology is the radius r.

The microstructure generated will be capable of adjustment in order to analyze quantified overall porosity together with any locally targeted porosity (which can be termed a porosity distribution function). This is attainable through the utilization of a Gaussian filter distribution. On the premise that the Gaussian filter is separable and could be utilized for every successful spatial direction; this study then utilized the logarithms to process pore radii as a replacement of the radii themselves and it was given for 1-D Gaussian as Eq. (1) (Altschuh et al., 2017). The parameters of the Gaussian filter distribution were determined based on the grouped quartiles analysis.

$$N(\mu,\sigma^2) = \frac{1}{\sigma\sqrt{2\pi}} e^{-\frac{(x-\mu)}{2\sigma^2}} \tag{1}$$

The cumulative distribution function for a function with normal distribution is given as:

$$\varphi(x) = \frac{1}{2}\left(1 + erf\left(\frac{x-\mu}{\sigma\sqrt{2}}\right)\right) \tag{2}$$

Where erf is the error function

$$erf(z) = \frac{2}{\sqrt{\pi}}\int_0^2 e^{-x^2} dx \tag{3}$$

X = normal random variable, i.e., X~N (μ, σ^2)

Where x represents the distance from the observed center point, σ (sigma) represents the standard deviation of the pore radius population and μ represents the population mean of the normal distribution.

2.9. Permeation, rejection and adsorption study

The permeate flux and rejection of iron and anions together with adsorption were studied as a function of time. The rejection, which is the measure of how well a membrane retains a solute, was calculated by Eq. (4). While the permeate flux Jv (L/m^2 /hr) was studied by taking the measurement of the volume of permeate collected in a given time interval divided by the membrane area (A) by using Eq. (5). The temperature of the flux was normalized by temperature correction factors.

$$\%\mathrm{Re} = \left(1 - \frac{C_p}{C_f}\right) \times 100 \tag{4}$$

$$J_v = \frac{Q}{A} \tag{5}$$

where C_p and $C_f$are the concentrations of anions and cation in the permeate and feed (mgL^{-1}) and*%Re* represent the percentage rejection.

In the isothermal adsorption study, all the anions and iron were studied using their initial concentrations in the river water. The adsorption capacity of the membranes was computed using Eq. (6).

$$Q_t = \frac{V(C_o - C_t)}{m} \tag{6}$$

$Q_t$in mg g^{-1} is the adsorption amount of the anions and cations at different time t, $C_0$is the initial concentration in mgL^{-1} and $C_t$is the concentrations (mgL^{-1}) at time t, V (L) is the volume of the solution and m (g) is the mass of the membrane.

3. Results and discussion

3.1. BET surface analysis of synthesized go and membranes

BET surface analysis is a very valuable measurement for the surface area and porosity of many synthesized materials. The surface area to volume ratio of nanomaterial significantly contributes to the determination of properties of synthesized materials. The pore size distribution and the reactive surface area of the GO were analyzed by adsorption/desorption under N_2 at a bath temperature of 77.4 K and ambient temperature of 295.15 K by BET measurement. The Brunauer-Emmett-

Teller of GO surface area and pore size volume of GO are depicted in Fig. 3. The total active specific surface area of GO is 332.850 m^2g^{-1}. The adsorption and desorption cumulative surface area of the pore was calculated by the Barrett-Joyner-Halenda method from the nitrogen curve to be 17.000 Å. The cumulative pore volume of the GO is 0.453300 cm^3g^{-1} (Fig. 3b), respectively. The pore size distribution of GO depicted that in nature, the material is porous with a hysteresis loop at elevated partial pressure (Nethravathi et al., 2014; Paranthaman et al., 2018). The graphene oxide exhibited a high surface area owing to the presence of interconnected pore networks.

3.2. SEM/EDX study

The morphological structure of the PET-graphene oxide nanocomposite membranes was analyzed using SEM. Fig. 4 shows PET-graphene oxide nanocomposite membranes with (a) having GO 1 wt.% incorporated in 20 wt.% PET and 10 wt.% PEG, (b) having GO 2 wt.% incorporated in 20 wt.% PET and 10 wt.% PEG and (c) having GO 3 wt.% incorporated in 20 wt.% PET and 10 wt.% PEG. The surface morphologies of the three membranes are considerably different, i.e., the top surface of M1 is a denser membrane with few pores while M2 and M3 possess numerous pores. However, the morphology of the M3 membrane has a structure possessing an inter-winning fibrous network with numerous pores (Fig. 4c). It also has some wrinkled morphology added to the inter-winning fibrous network. In all, all the membranes demonstrate that they possess a porous support layer. Thus, these membranes are highly symmetric porous membranes with rigid, and they are highly voided with randomly distributed interconnected pores. Therefore, only molecules that are significantly variant in size would be separated efficiently by these membranes. In order to examine the number of elements of membranes, EDX was conducted. Fig. 5 depicts the EDX spectra of synthesized membranes and the alterations in the proportion of each element with respect to the amount of GO integrated into the membranes. From Fig. 5a, the 1 wt.% GO incorporated in 20 wt.% PET and 10 wt.% PEG showed a decreased atomic ratio of carbon and an increased atomic ratio of sulfur. The atomic ratio of carbon in the membranes increases with an increasing amount of GO while the atomic ratio of sulfur reduces with an increasing amount of GO (see Fig. 5a, b, and c) (Nguyen et al., 2019). In addition, the EDX spectrum of all the PET-graphene oxide nanocomposite membranes denotes carbon and oxygen peaks at 0.23 and 0.52 keV. A high peak for carbon is detected as a result of the higher carbon content that was more than oxygen in PET-graphene oxide nanocomposite membranes. This is in accordance with the study of Jang et al. (2020). These results showed that GO exists in the synthesized PET-GO nanocomposite membranes.

3.3. Pore size distribution of membranes from BET

Fig. 6 depicts the pore size distribution of PET-graphene oxide membranes. It was detected that the number of pore volume steadily reduces with an upsurge in the quantity of GO embedded in the membranes. It was also observed that, the more the quantity of GO embedded in the membrane the smaller the sizes of the pores. It further shows that the pore size distribution varies; this is confirmed in Fig. 6. In course of comparing the pore sizes of the membrane, Fig. 6 shows that an increase in the quantity of GO embedded in the membrane leads to more stable distribution of pore size. A smaller quantity of GO (1wt%) results in less stable pore size as the distribution (Suntornnond et al., 2016). As the pore width increased steadily, samples became more porous.

3.4. Statistical analyses

The features of membrane pore structures (pore size, pore size data distribution, and pore density) ought to be the strength of the membrane industry because these features support the filtration properties of membranes. Fig. 7 shows the distribution of subsequent probabilities of M1, M2 and M3 with Quartiles analysis using a NumPy. The quantiles are the set of values that divides the radius dataset into groups of four equal size. This framework is useful to draw a qualitative pore radius landscape, which will predict a minimum radius size for the filtration. Beyond that radius size; however, still within an intermediate size in the quartiles, the pore seems to have a tendency to shrink towards the right, since the data distribution towards the dominates lower frequency; hence distortion of skewness statistic was observed. These subsequent probabilities distribution data for the three membranes suggested that all the pores that will enable the anions and cations to pass through the membranes exhibited asymmetric distribution profiles; which is characterised by substantially tailing to the direction of higher permeability coefficient values. This is in accordance with the study of Frum et al. (2007) on the correlation between drug properties and in vitro transdermal flux variability. The areas with higher frequency for the three membranes serve as the critical radius that represents the active pore structure of the pore formation, which should be taken as the pore area for the membrane filtration.

The statistical analyses were further done on the assumption the variable (pore radius) x is assumed to be uniformly distributed if the density function is:

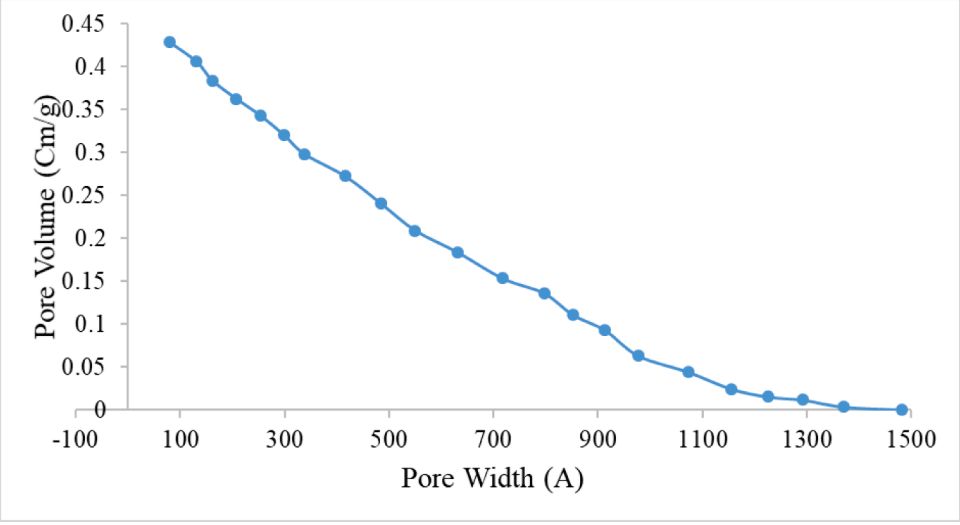

Fig. 3. Brunauer-Emmett-Teller of pore size volume of GO.

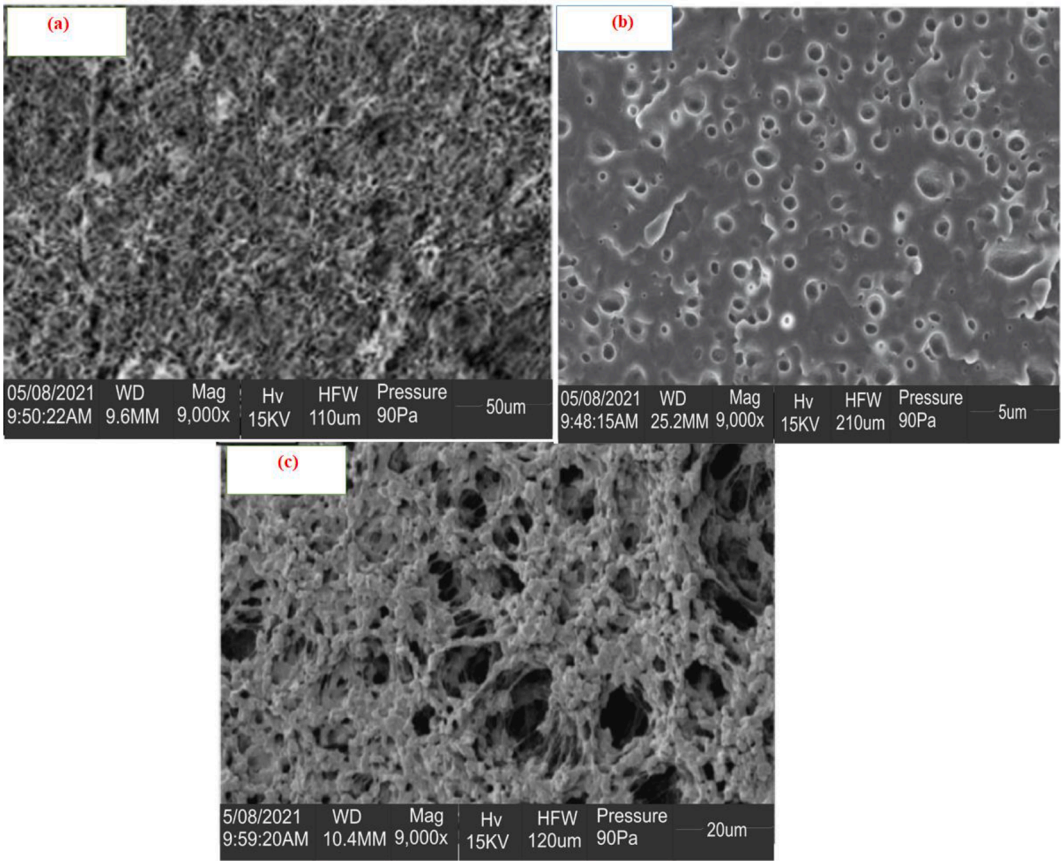

Fig. 4. SEM micrograph of PET-graphene oxide nanocomposite membranes; (a) - GO 1 wt.%, (b) - GO 2 wt.%, (c)-GO 3 wt.%.

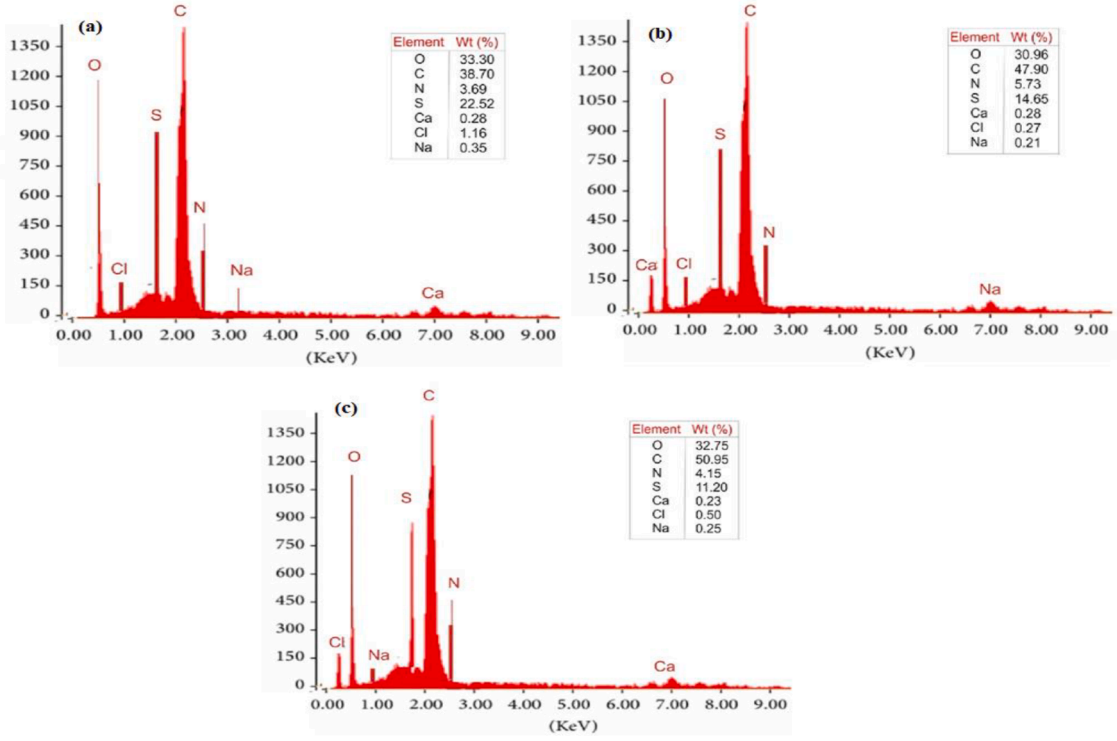

Fig. 5. EDX spectral of PET-graphene oxide nanocomposite membranes; (a) - GO 1 wt.%, (b) - GO 2 wt.%, (c)-GO 3 wt.%.

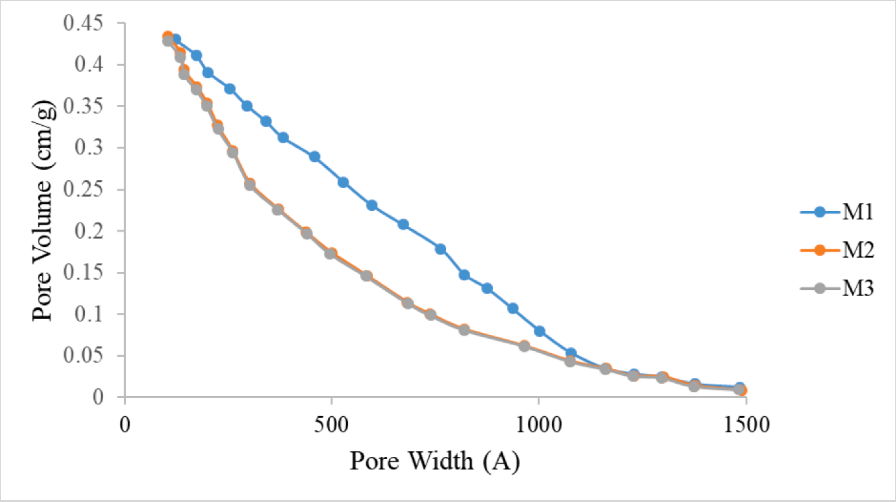

Fig. 6. Pore size distribution of PET-graphene oxide membranes (a) M1, (b) M2, (c) M3.

$$f(x) = \frac{1}{a-b} \tag{7}$$

For $-\infty < a \le x \le b < \infty$

The parameters of a standard uniform density are $a = 0$ and $b = 1$; hence, the probability density function for standard uniform density is expresses as:

$$f(x) = \left\{ \begin{matrix} 1, 0 \le x \le 1 \\ 0, otherwise \end{matrix} \right\} \tag{8}$$

The data distribution of the membrane pores shown in Fig. 8 depicted that pore size distribution on the membranes is another factor that could have an impact on the reliability of membrane separation. The data distribution is in conformity with Fig. 6 which depicted that an upsurge in the quantity of GO integrated into the membrane resulted in more stable distribution of pore size. Smaller quantity of GO (1wt%) results in lesser distribution of data. However, it can be observed that the shape of the uniform distribution curve is rectangular for the three membranes. This also confirms that the skewness statistic enumerates the degree of symmetry of a distribution around its mean. As observed in Fig 8, this ranged from zero for a perfectly symmetrical distribution to progressively larger values with a positive skewness; which is the heavier tailing on the right-hand side of the distribution observed in Fig. 7. This is also in conformity with the study of Frum et al. (2007). For uniform distribution, **a** and **b** are the parameters.

Pore size and pore radii distributions are very significant parameters used for data analysis in membrane technology. They provide a measurable depiction of the span of pore sizes existing in a particular membrane and they provide an added precise depiction of the particle sizes and radii that are probably to be retained by the membranes (Agboola et al., 2015). Fig. 9 shows the distribution of the mean of M1, M2, and M3 using the pore radii data via the central tendency. Central tendency infers the propensity of the data points to cluster around their central value. The two most commonly used measures of central tendency are mean and median. Central tendency pronounces the distance in which the horizon that is away from the radius data points is likely to fall from the center. The figure shows that the radius data distribution is firmly clustered around the mean with M1 having the of 2.5, M2 having the mean of 0.25, and M3 having the mean of 0.35. This shows that the more the graphene oxide is embedded in the membrane the lesser the value of the mean. Furthermore, in statistics, the mean summarizes a whole dataset with a single number representing the data's typical value or the center point. Hence, a low value observed in M3 shows that there is a high degree of confidence that the membrane will produce consistent permeate when compared to the other membranes. Thus, the permeate from the system can be approximated by a mean value devoid of the necessity to justify and give account for important variability owing to the membrane fabrication process (Sharma, 2018).

Fig. 10 shows the distribution of the membranes microstructures of the three membranes. It reflects the averages of microstructures with respect to the aforementioned objects (mean and pore radius). Hence, in order to analyze the impact of porosity on the membrane filtration, the averages of the microstructure for each porosity value specified in the microstructure generated were analyzed by employing an evenly distribution curve and mean. It shows that the porosity increases with an increasing quantity of GO. As stated earlier, the mean and mode relate to the direct characteristics of the membrane microstructure. This is in good accordance with the pose size distribution depicted in Fig. 6. It is also evidently observed that the upsurge in porosity resulted in larger frequency values. Furthermore, the horizontal-like vacancies between the clusters histogram of Fig. 10 are in correspondence to porosities between the values obtained from the distribution in Fig. 9 of the distribution of mean used in the microstructure generation. Furthermore, the effect of the number of pores used in microstructure generation is depicted in the bottom row of Fig. 10. It was presumed that a microstructure was shifted towards the higher value of the distribution which is correlated with more distribution of pore sizes observed in M2 and M3. This is in accordance with the study of Altschuh et al. (2017). However, their study used a microstructure generator and employed it to generate a large ensemble of porous structures covering a considerable series in measures of structures such as the stretched pore shapes, porosity, specific surface, and pore sizes.

3.5. Evaluation of membrane performance

The increase in the ratio of GO embedded in the PET membranes induces less water flux and a higher rejection rate (See Figs. 11 and 12). This is in conformity with the data generated from the statistical analysis. The% rejection of the three membranes increases with an increase in time. M3 membrane has a higher rate of rejection for NO^{3-}, Cl^{-}, HCO^{3-} and Fe. Although, rejection can differ in proportion to the water chemistry, temperature, pressure, feed flow rate, pH, etc. Hence, the percentage rejection anions and cation with M3 membrane is 96%, 85 %, 72%, and 60% respectively for NO^{3-}, Cl^{-}, HCO^{3-} and Fe. In addition, the high rejection of anions was due to the decrease in the membrane pore size; this is confirmed by the pore sizes obtained from ImageJ studies. However, the low rejections of Fe can be accredited to the decreased concentration of the Fe at the phase of the membrane. This takes place in mixtures of electrolytes on the account of the speeding up of such ions by the electric field of diffusion potential coming up owing

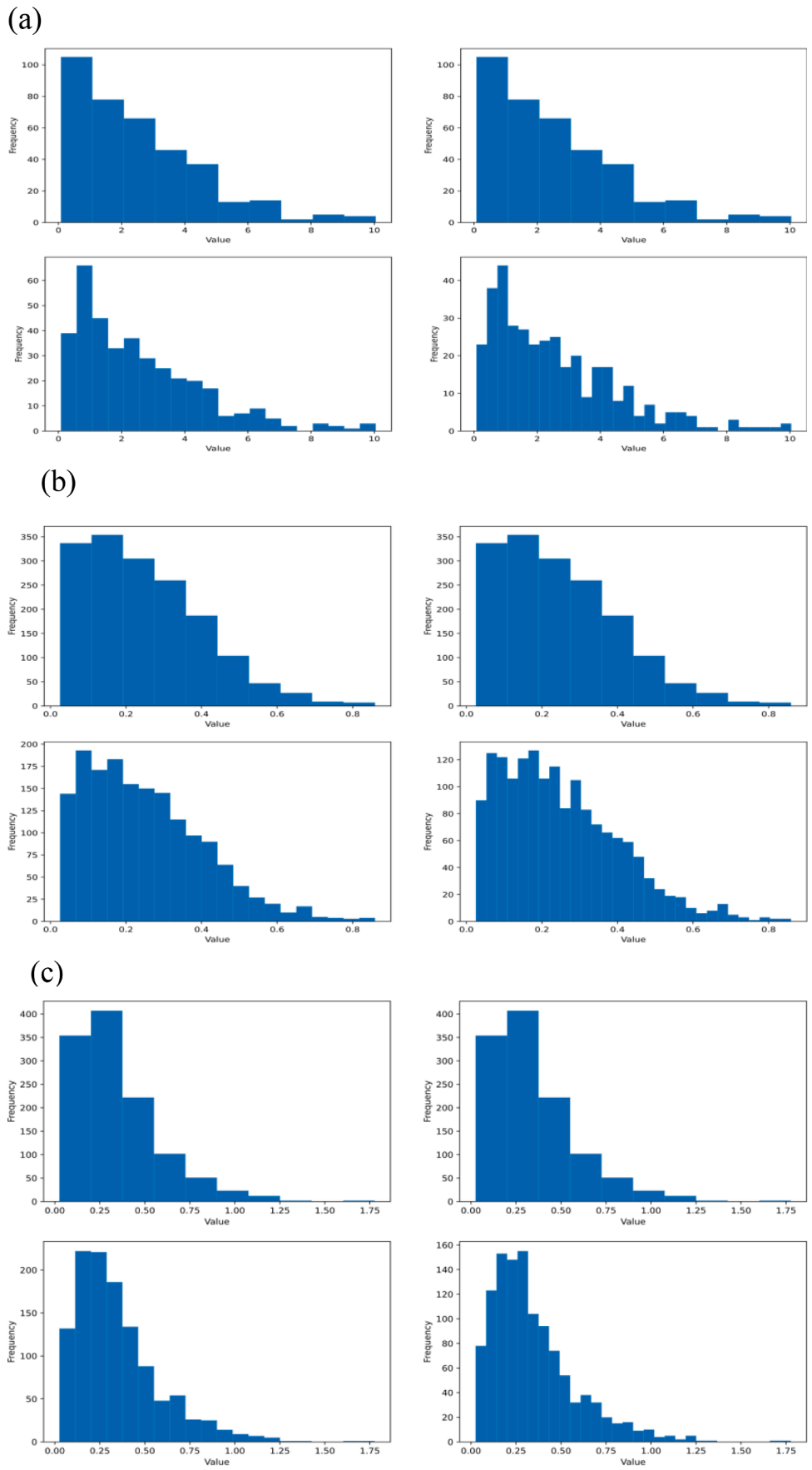

Fig. 7. Distribution of subsequent probabilities of M1 (a), M2 (b) and M3 (c) with quartiles analysis using a NumPy.

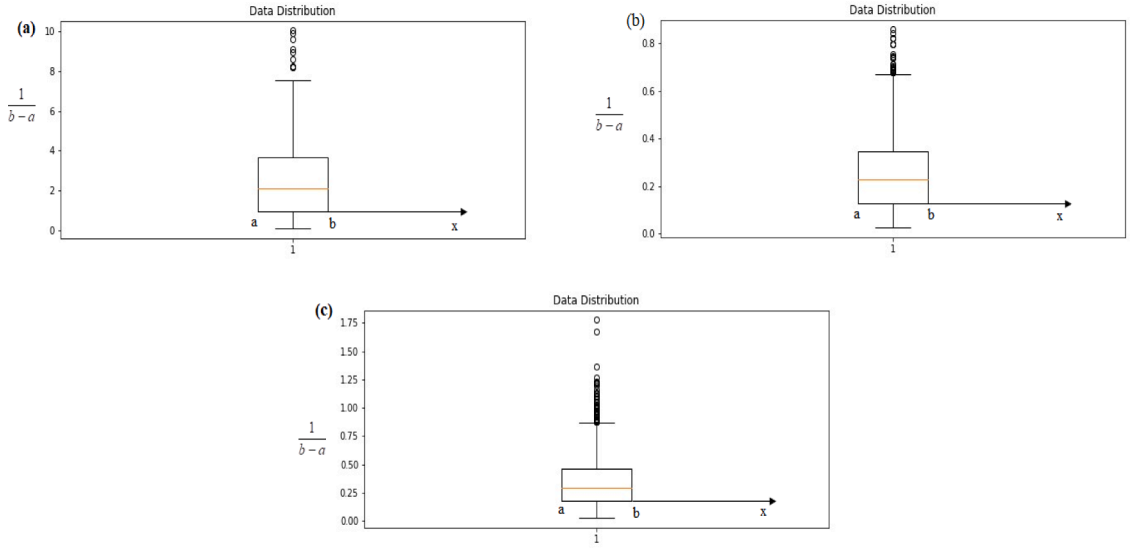

Fig. 8. The radius of pore distribution of PET-graphene oxide membranes (a) M1, (b) M2, (c) M3.

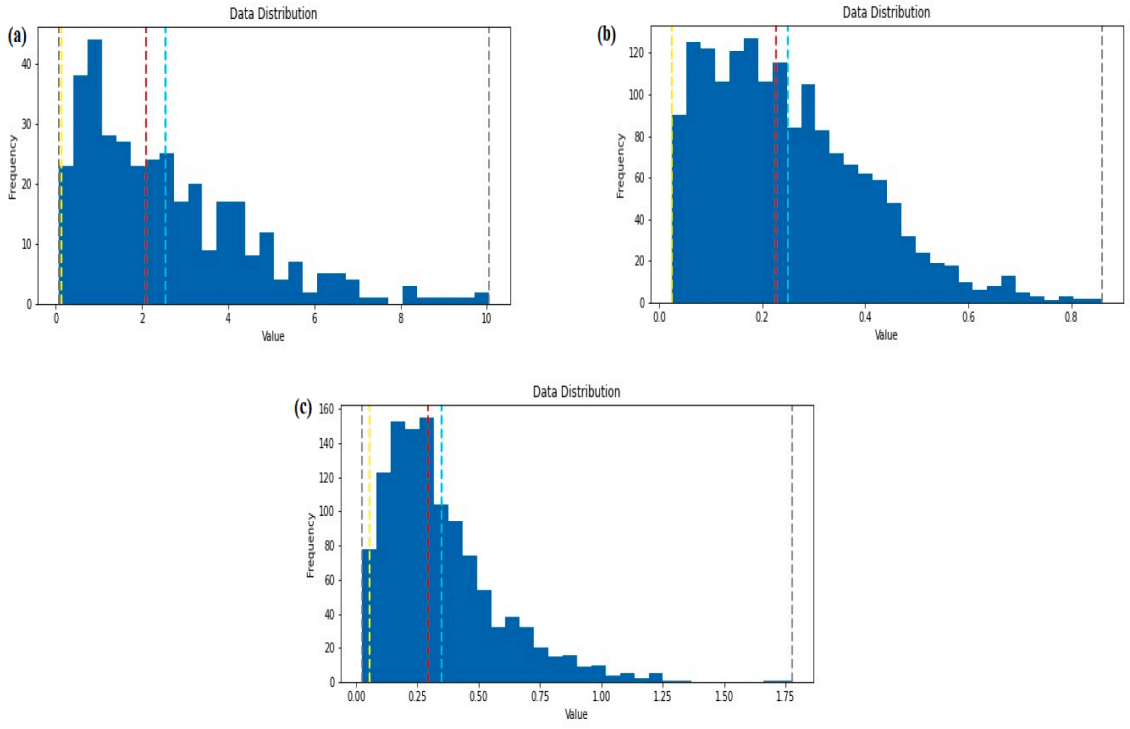

Fig. 9. The distribution of PET-graphene oxide membranes (a) M1, (b) M2, (c) M3, showing the mean and mode of pore radius.

to strong rejections of other mixture components (Yaroshchuk 2008). Furthermore, the results show that the variance of the dielectric constant inside the membranes pore was significant. It is of the opinion that when the dielectric constant inside the pores declines, it becomes smaller than the bulk solution dielectric exclusion. Thus, alterations of the dielectric constant in the pores prompted an additional energy barrier for ion solvation, averting charged ions from penetrating into the pores; Hence, the lower rejection of Fe. The dielectric exclusion (DE) was responsible for this effect (Suhalim et al., 2022). Furtherance to this discussion, literature has it that when a certain feed solution that is made of both positively charged ions (such as Fe^{2+}) and negatively charged ions (such as NO^{3-}, Cl^{-}, HCO^{3-}) come in contact with a negatively charged membrane, the concentration of cations on the surface of the membrane would be greater than their concentration in the bulk solution. Concurrently, the concentration of anions on the surface of the membrane turns out to be less than the concentration in the bulk solution. Such an ion shift generates an electrical potential called the Donnan potential at the border between the membrane and the solution. Therefore, the Donnan potential has the capacity to draw cations to the membranes while repelling anions; resulting in the upsurge of anions rejection (Bartels et al., 2005). These facts validate the result obtained in Fig. 11.

Lower flux ensued as a result of aggregation in the course of membrane synthesis which causes a reduction in the number of pores (see Fig. 6a). This was also confirmed in Fig. 10, showing tightly clustered radius data distribution around the mean. Hence, the lack of aggregation

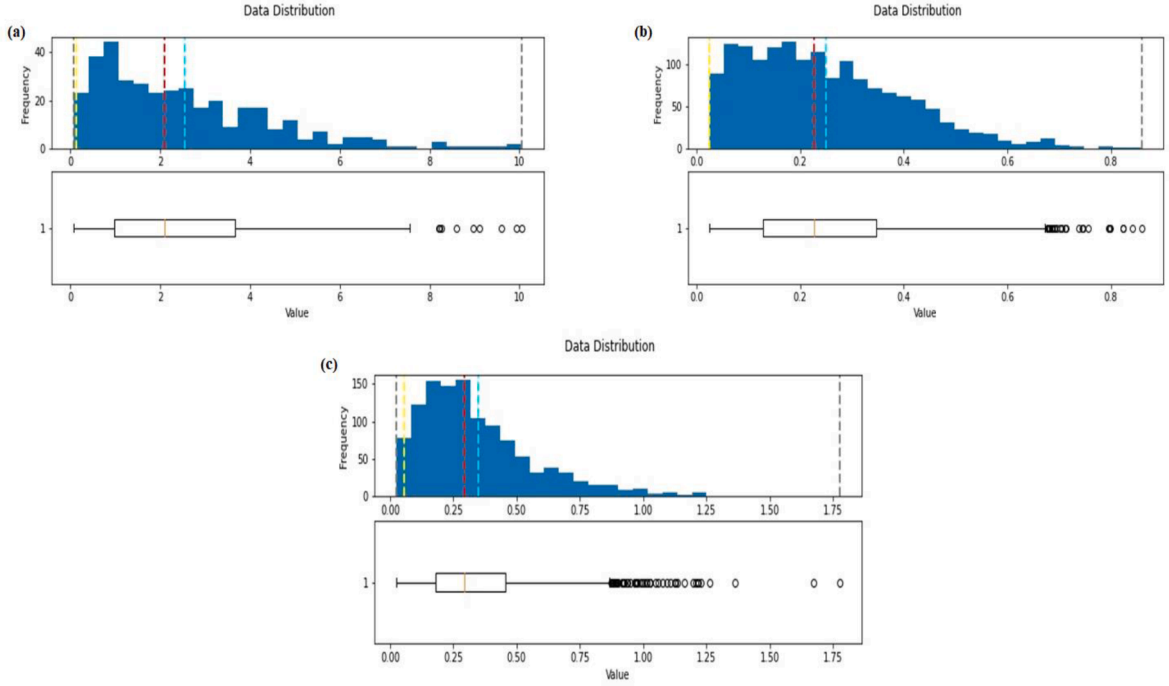

Fig. 10. Distribution of the membranes microstructures with respect to the mean and the radius pore distribution of (a) M1, (b) M2, (c) M3.

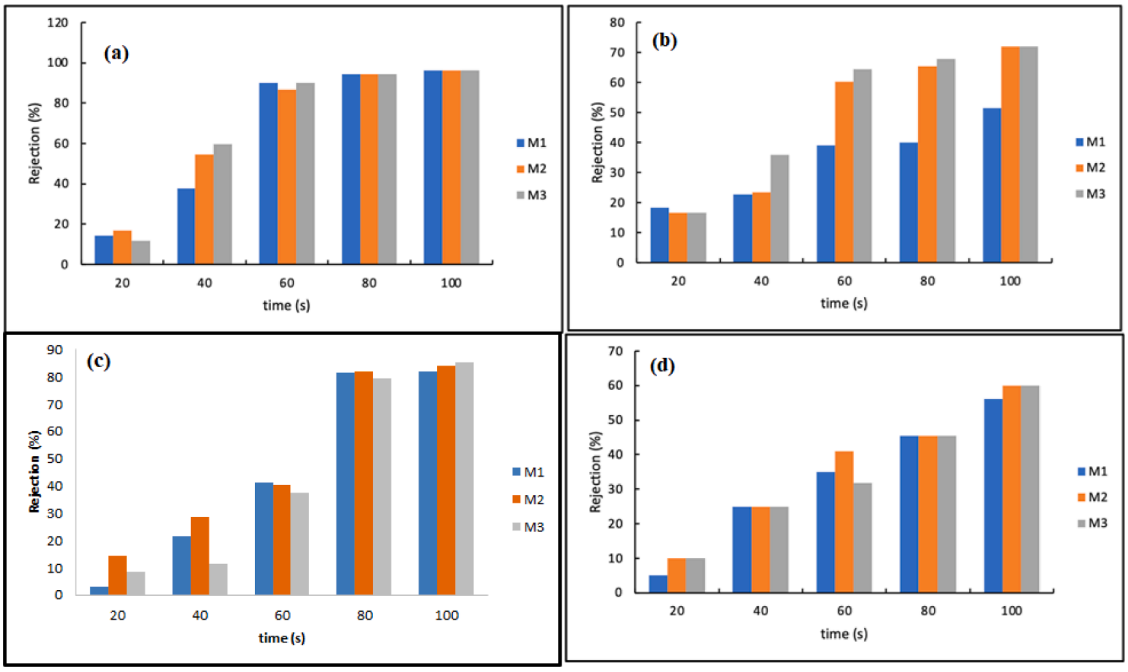

Fig. 11. Rejection of (a) (NO^{3-}) anion, (b) (Cl^{-}) anion, (c) (HCO^{3-}) anion and (d) Fe cation.

can occur when the low probability of the GO particles approaches shorter distances due to the impact spawned by the PET-graphene oxide nanocomposite membranes matrix (Dukhin and Goetz 2017). Furthermore, PET-graphene oxide nanocomposite membranes with 3wt% GO showed higher porosity, which is demonstrated in the SEM image and the pore size distribution (see Figs. 4c and 6c); hence, with the 3wt% GO, a maximum water flux was reached (see Fig. 12). The further upsurge in the amount of GO (2wt% and 3wt%) resulted in an upsurge of the water flux. This is in conformity with the mean statistic obtained in Fig. 9. It is also in accordance with the study of Jalali et al. (2019); from their study, flux was improved with the incorporation of graphene oxide. The transport mechanism responsible for the reduction in flux in this study is the pore size of the membranes. The transport description responsible for this mechanism is inserted in Fig. 12. This description shows that pore blockage occurred; hence, the reduction in flux.

The concentrations of anions and iron obtained per time of filtration of the river water were used in the adsorption study. The effect of adsorption in Fig. 13 showed that the adsorption increases with time. The adsorption sites of the membranes three were not all occupied at the initial stage of adsorption (at 20 min) (Tang et al., 2019); hence, lower

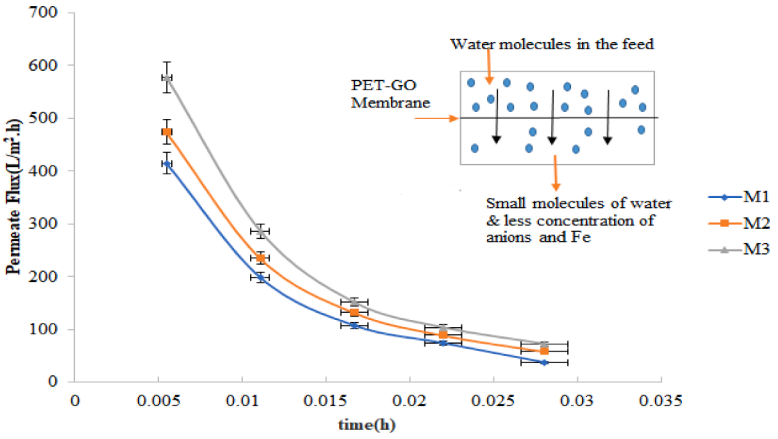

Fig. 12. Normalized flux from the PET-graphene oxide nanocomposite membranes.

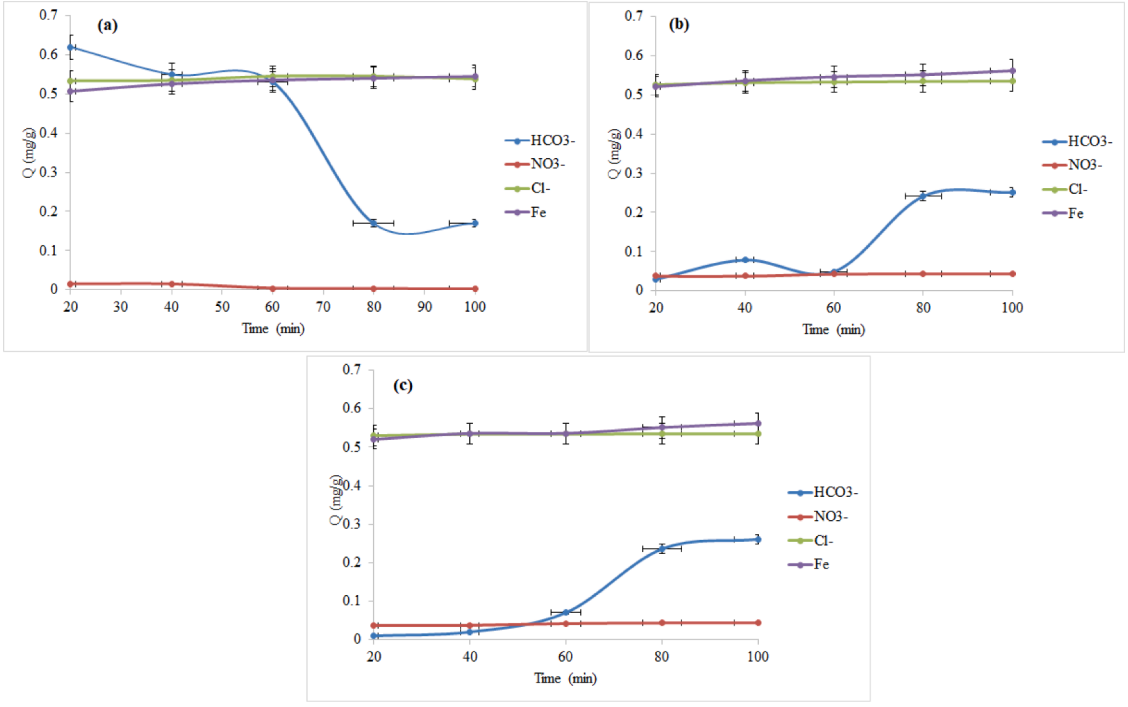

Fig. 13. Effect of the iron and anions adsorption time on adsorption capacity.

adsorption at that time. The molecules of the anions and iron quickly combined with the adsorption sites as the time increased; thus, the adsorption rate was fast with time. The adsorption capacity of M1 membrane depicts a lower capacity than that of M2 and M3 membranes. This is accredited to the increase in the integration of GO in the PET polymer resulting in better adsorption capacity; which aided the accumulation of water film on the membrane. The nitrate, chlorine, and iron reached equilibrium at 80 min except for bicarbonate ions. This could be a result of the affinity of the anions. Anion affinity can be defined as the power of a cation to attract anions in the transitory state at the surface of the membrane and the ionization potential is employed as a comparative measure of anion affinity (Ahrens, 1953). Hence, Fe does not have the power to attract HCO^{3-} in the transitory state at the surface of the membrane; thus HCO^{3-} could not reach equilibrium.

4. Conclusion

PET-graphene oxide nanocomposite membranes were fabricated via non-solvent-induced phase separation on a support (nonwoven polyester material) by employing polyethylene glycol as an additive. Increasing the amount of GO in the course of fabrication resulted in a reduction in the membrane pore sizes. The effective surface porosity increased with an increase in the quantity of GO embedded in the membrane. The pore size distribution was studied using BET. The statistical study was done via Gaussian filter distribution by using quartiles analysis. The mean and mode were regarded as the best measure of central tendency as it contains all the features of an ideal microstructure measure. The radius data distribution was firmly clustered around the mean. The composite ratio of GO in PET has an impact on the rejection and flux behavior of the membranes for iron and anions removal from Ibeshe river water. The study has established that the association of PET with GO to make nanocomposites membranes is a promising means of attaining membranes with better performances; as a higher rejection rate was attained. In addition, statistics obtained showed that Gaussian distribution using Quartiles analysis is an effective method that relates to the study of permeate flux through the pore radii.

Data availability statement

All data generated or analysed in the course of this study will be provided upon request.

Source of funding

The authors declare that no funds of grant were received in the course of preparing this manuscript.

CRediT authorship contribution statement

Oluranti Agboola: Conceptualization, Supervision. **Ajibola Ademola Khalih:** Investigation, Methodology. **Olagoke Oladokun:** Formal analysis, Software. **Augustine Omoniyi Ayeni:** Validation. **Frederick Chukwudubem Uzokwe:** Visualization. **Olayemi Odunlami:** Writing – original draft. **Francis Eleninafe:** Writing – review & editing. **Abdulrazaq Yahaya:** Writing – review & editing. **Ojo Sunday Isaac Fayomi:** Writing – review & editing.

Declaration of Competing Interest

The authors declare that we have no known competing interests with regard to finance and personal relationships that could have appeared to influence the work reported in this paper.

Acknowledgments

The authors acknowledge Covenant University for providing financial support for the publication of this manuscript.

References

Agboola, O., Fayomi, O.S.I., Ayoola, A., Ayeni, A.O., Alagbe, E.E., Sanni, S.E., Okoro, E. E., Moropeng, L., Sadiku, R., Kupolati, W.K., Oni, B.A., 2021. A Review on polymer nanocomposites and their effective applications in membranes and adsorbents for water treatment and gas separation. Membranes 11 (139), 1–33.

Agboola, O., Maree, J., Mbaya, R., 2014. Characterization and performance of nanofiltration membranes. Environ. Chem. Lett. 12, 241–255.

Agboola, O., Maree, J., Mbaya, R., Kolesnikov, A., Sadiku, R., Verliefde, A., D'Haese, A., 2015. Microscopical characterization of nanofiltration membranes for the removal of nickel ion from aqueous solution. Korean J. Chem. Eng. 32 (4), 731–742.

Agboola, O., Sadiku, E.R., 2014. Theoretical modeling of nanostructured formation of polymer blends. Nanostructured Polymer Blends. Elsevier, p. 37.

Ahrens, L.H., 1953. The use of ionization potentials Part 2. Anion affinity and geochemistry. Geochim. Cosmochim. Acta 3 (1), 1–29.

Altschuh, P., Yabansu, Y.C., Hötzer, J., Selzer, M., Nestler, B., Kalidindi, S.R., 2017. Data science approaches for microstructure quantification and feature identification in porous membranes. J. Membr. Sci. 540, 88–97.

Bartels, C., Franks, R., Rybar, S., Schierach, M., Wilf, M., 2005. The effect of feed ionic strength on salt passage through reverse osmosis membranes. Desalination 184, 185–195.

Bayat, S., Moini Jazani, O., Molla-Abbasi, P., Jouyandeh, M., Saeb, M.R., 2019. Thin films of epoxy adhesives containing recycled polymers and graphene oxide nanoflakes for metal/polymer composite interface. Prog. Org. Coat. 136, 105201.

Beita-Sandí, W., Karanil, T., 2017. Removal of both N-nitrosodimethylamine and trihalomethanes precursors in a single treatment using ion exchange resins. Water Res. 124, 20–28.

Bethi, B., Sonawane, S.H., Bhanvase, B.A., Gumfekar, S.P., 2016. Nanomaterials based advanced oxidation processes for wastewater treatment: a review. Chem. Engin. Process. 109, 178–189.

Carr, S.A., Liu, J., Tesoro, A.G., 2016. Transport and fate of microplastic particles in wastewater treatment plants. Water Res. 91, 174–182.

De-Meis, D. 2017. Overview on porous inorganic membranes for gas separation. RT/2017/5/ENEA, (Retrieved 25th January 2022).

Department of natural resources, Iron in drinking water. 2017. https://dnr.wi.gov/files/pdf/pubs/dg/dg0035.pdf [Assessed 24th March 2022].

Diaz-Reinoso, B., 2020. Chapter 14 - concentration and purification of seaweed extracts using membrane technologies. Sustainable Seaweed Technologies. Elsevier, pp. 371–390.

Dukhin, A.S., Goetz, P.J., 2017. Characterization of Liquids, Dispersions, Emulsions and Porous Materials Using Ultrasound, 33rd Edition. Elsevier.

Dunning, H., 2020. Size Determines How Nanoparticles Affect Biological Membranes. Imperial College, London. https://www.imperial.ac.uk/news/204433/size-determines-nanoparticles-affect-biological-membranes/#:~:text=They%20found%20that%20larger%20nanoparticles,distorted%20the%20membrane%2C%20bending%20it [Retrieved 24th January 2022].

Elessawy, N.A., Gouda, M.H., Elnouby, M., Ali, S.M., Salerno, M., Youssef, M.E., 2022. Sustainable microbial and heavy metal reduction in water purification systems based on PVA/IC nanofiber membrane doped with PANI/GO. Polymers (Basel) 14, 1–16, 1558.

Flory, P.J., 1942. Physical chemistry of polymers: thermodynamics of high polymer solutions. J. Chem. Phys. 10, 51–61.

Flory, P.J., Krigbaum, W.R., 1950. Statistical mechanics of dilute polymer solutions. J. Chem. Phys. 18, 1086–1094.

Frum, Y., Khan, G.M., Sefcik, J., Rouse, J., Eccleston, G.M., Meidan, V.M., 2007. Towards a correlation between drug properties and in vitro transdermal flux variability. Int. J. Pharma. 336, 140–147.

Gadde, U.W., 1999. Polymer Physics. Kluwer, Dordrecht.

Gaouar, M.Y., Benguella, B., 2016. Efficient and eco-friendly adsorption using low-cost natural sorbents in wastewater treatment. Indian J. Chem. Technol. 23, 204–209.

Goh, P.S., Othman, M.H.D., Matsuura, T., 2021. Waste reutilization in polymeric membrane fabrication: a new direction in membranes for separation. Membrane 11, 782.

Gu, B., Renaud, D.L., Sanaei, P., Kondic, L., Cummings, L.J., 2020. On the influence of pore connectivity on performance of membrane filters. J. Fluid Mech. 902, 1–33.

Huang, K., Liu, G., Lou, Y., Dong, Z., Shen, J., Jin, W., 2014. A graphene oxide membrane with highly selective molecular separation of aqueous organic solution. Angew. Chem. 53, 6929–6932.

Jalali, S., Mehrabadi, A.R., Shayegan, J., Mirabi, M., Madaeni, S.S., 2019. Flux enhancement of thin film composite membrane by graphene oxide incorporation. J. Environ. Health Sci. Eng. 17, 377–382.

Jang, J., Park, I., Chee, S.-S., Song, J.-H., Kang, Y., Lee, C., Lee, W., Ham, M.-H., Kim, I. S., 2020. Graphene oxide nanocomposite membrane cooperatively cross-linked by monomer and polymer overcoming the trade-off between flux and rejection in forward osmosis. J. Membr. Sci. 598, 117684.

Khalifa, R.E., Omer, A.M., Abd Elmageed, M.H., Mohy Eld, M.S., 2021. Titanium dioxide/phosphorous-functionalized cellulose acetate nanocomposite membranes for DMFC applications: enhancing properties and performance. ACS Omega 6, 17194–17202.

Kim, Y., Rana, D., Matsuura, T., Chung, W.-J., 2009. Influence of surface modifying macromolecules on the surface properties of poly(ether sulfone) ultrafiltration membranes. J. Membr. Sci. 338, 84–91.

Kim, Y., Rana, D., Matsuura, T., Chung, W.-J., 2012. Towards antibiofouling ultrafiltration membranes by blending silver containing surface modifying macromolecules. Chem. Commun. 48, 693–695.

Kim, Y., Rana, D., Matsuura, T., Chung, W.-J., Khulbe, K.C., 2010. Relationship between surface structure and separation performance of poly(ether sulfone) ultra-filtration membranes blended with surface modifying macromolecules. Sep. Purif. Technol. 72, 123–132.

Koningsveld, R., Kleintjens, L.A., Schoffeleers, H.M., 1974. Thermodynamic aspects of polymer compatibility. Pure Appl. Chem. 39, 1–32.

Lawal, A.T., 2020. Recent progress in graphene based polymer nanocomposites. Cogent Chem. 6, 1–50.

Li, X., Li, J., Fang, X., Bakzhan, K., Wang, L., Van der Bruggen, B., 2016. A synergetic analysis method for antifouling behavior investigation on PES ultrafiltration membrane with self-assembled TiO_2 nanoparticles. J. Colloid Interface Sci. 469, 164–176.

Li, Y.-Y., Gurkan, B., 2021. Graphene oxide reinforced facilitated transport membrane with poly(ionic liquid) and ionic liquid carriers for CO_2/N_2 separation. J. Membr. Sci. 638, 119652.

Liang, Y., Li, C., Li, S., Su, B., Hu, M.Z., Gao, X., Gao, C., 2020. Graphene quantum dots (GQDs)-polyethyleneimine as interlayer for the fabrication of high performance organic solvent nanofiltration (OSN) membranes. Chem. Eng. J. 380, 122462.

Longs Ecowater. 2022. What are the effects of iron in water? https://longsecowater.com/ [Assessed 23rd March 2022].

Luo, M., Wen, Q., Liu, J., Liu, H., Jia, Z., 2011. Fabrication of SPES/Nano-TiO_2 composite ultrafiltration membrane and its anti-fouling mechanism. Chinese J. Chem. Eng. 19, 45–51.

Mansoori, S., Davarnejad, R., Matsuura, T., Ismail, A.F., 2020. Membranes based on non-synthetic (natural) polymers for wastewater treatment. Polym. Test 84, 106381.

Maráková, N., Boeva, Z.A., Humpolíček, P., Lindfors, T., Pacherník, J., Kašpárková, V., Radaszkiewicz, K.A., Capáková, Z., Minařík, A., Lehocký, M., 2019. Electrochemically prepared composites of graphene oxide and conducting polymers: cytocompatibility of cardiomyocytes and neural progenitors. Mater. Sci. Eng: C 105, 110029.

Nethravathi, C., Rajamathi, C.R., Rajamathi, M., Wang, X., Gautam, U.K., Golberg, D.M., Bando, Y., 2014. Cobalt hydroxide/oxide hexagonal ring-graphene hybrids through chemical etching of metal hydroxide platelets by graphene oxide: energy storage applications. ACS Nano 8, 2755–2765.

Nguyen, H.T.V., Ngo, T.H.A., Do, K.D., Nguyen, M.N., Dang, N.T.T., Nguyen, T.T.H., Vien, V., Vu, T.A., 2019. Preparation and characterization of a hydrophilic polysulfone membrane using graphene oxide. J. Chem. 1–11.

Oluwafemi, A.M. 2018. The Lagos water crisis: any role for the private sector?-Urbanet, https://www.urbanet.info/nigeria-lagos-water-crisis/ [Retrieved 19th January 2022].

Paranthaman, V., Sundaramoorthy, K., Chandra, B., Pandian, S., Alagarsamy, M.P., Perumalsamy, R., 2018. Investigation on the performance of reduced graphene oxide as counter electrode in dye sensitized solar cell applications. Phys. Status Solidi A 215, 1–9.

Patel, S.H., Xanthos, M., 2001. Environmental Issues in Polymer Processing: A Review on Volatile Emissions and Material/Energy Recovery Options, 20. Springer, Berlin/Heidelberg, Germany.
Paulchamy, B., Arthi, G., Lignesh, B.D., 2015. A simple approach to stepwise synthesis of graphene oxide nanomaterial. J. Nanomed. Nanotechnol. 6, 1–4.
Pulido, B.A., Habboub, O.S., Aristizabal, S.L., Szekely, A.G., Nunes, S.P., 2019. Recycled poly(ethylene terephthalate) for high temperature solvent resistant membranes. ACS Appl. Polym. Mater. 9, 2379–2387.
Rana, D., Bag, K., Bhattacharyya, S.N., Mandal, B.M., 2000. Miscibility of poly(styrene-co-butyl acrylate) with poly(ethyl methacrylate): existence of both UCST and LCST. J. Polym. Sci. Polym. Phys. Ed. 38 (3), 369–375.
Rana, D., Mandal, B.M., Bhattacharyya, S.N., 1993. Miscibility and phase diagrams of poly (phenyl acrylate) and poly(styrene-co-acrylonitrile). Polymer (Guildf) 34 (7), 1454–1459.
Rana, D., Mandal, B.M., Bhattacharyya, S.N., 1996. Analogue calorimetry of polymer blends: poly(styrene-co-acrylonitrile) and poly (phenyl acrylate) or poly(vinyl benzoate). Polymer (Guildf) 34 (12), 2439–2443.
Sali, S., Mackey, H.R., Abdala, A.A., 2019. Effect of graphene oxide synthesis method on properties and performance of polysulfone-graphene oxide mixed matrix membranes. Nanomaterials 9, 1–16.
Sharma A. 2018. Porous anodic alumina membranes for large biomolecule separations. PhD Thesis, University College London.
Suhalim, N.S., Kasim, N., Mahmoudi, E., Shamsudin, I.J., Mohammad, A.W., Zuki, F.M., Jamari, N.L.-A., 2022. Rejection mechanism of ionic solute removal by nanofiltration membranes: an overview. Nanomaterials 12, 1–18.
Suntornnond, R., An, J., Tijore, A., Leang, K.F., Chua, C.K., Tan, L.P., 2016. A solvent-free surface suspension melt technique for making biodegradable PCL membrane scaffolds for tissue engineering applications. Molecules 21, 1–13.
Tang, Q., Li, N., Lu, Q., Wang, X., Zhu, Y., 2019. Study on preparation and separation and adsorption performance of knitted tube composite-cyclodextrin/chitosan porous membrane. Polymers (Basel) 11, 1–17.
Tran, B.N., Thickett, S.C., Agarwal, V., Zetterlund, P.B., 2021. Influence of polymer matrix on polymer/graphene oxide nanocomposite intrinsic properties. Appl. Polym. Mater. 3, 5145–5154.
Wu, Z., Zhang, C., Peng, K., Wang, Q., Wang, Z., 2018. Hydrophilic/underwater superoleophobic graphene oxide membrane intercalated by TiO_2 nanotubes for oil/water separation. Front. Environ. Sci. Eng. 12, 1–10.
Yang, Y., Pignatello, J.J., Ma, J., Mitch, W.A., 2016. Effect of matrix components on UV/H_2O_2 and UV/SO_2 advanced oxidation processes for trace organic degradation in reverse osmosis 28 brines from municipal wastewater reuse facilities. Water Res. 89, 192–200.
Yaroshchuk, A.E., 2008. Negative rejection of ions in pressure-driven membrane processes. Adv. Colloid Interface Sci. 139, 150–173.
Younas, H., Bai, H., Shao, J., Han, Q., Ling, Y., He, Y., 2017. Super-hydrophilic and fouling resistant PVDF ultrafiltration membranes based on a facile prefabricated surface. J. Membr. Sci. 541, 529–540.
Zhang, H.-.B., Zheng, W.-.G., Yan, Q., Yang, Y., Wang, J.-.W., Lu, Z.- H., Ji, G.-.Y., Yu, Z.-.Z., 2010. Electrically conductive polyethylene terephthalate/graphene nanocomposites prepared by melt compounding. Polymer (Guildf) 51 (5), 1191–1196.
Zhao, S., Wang, P., Wang, C., Sun, X., Zhang, L., 2012. Thermostable PPESK/TiO_2 nanocomposite ultrafiltration membrane for high temperature condensed water treatment. Desalination 299, 35–43.
Zinadini, S., Zinatizadeh, A.A., Rahimi, M., Vantapour, V., Zangene, H., 2014. Preparation of a novel antifouling mixed matrix PES membrane by embedding graphene oxide nanoplates. J. Membr. Sci. 453, 292–301.